Detection of burning ashes from thermonuclear X-ray bursts

J. J. E. Kajava,[1]⋆ J. Nättilä,[2,3] J. Poutanen,[2,3] A. Cumming,[4] V. Suleimanov[5,6] and E. Kuulkers[1]

[1]*European Space Astronomy Centre (ESA/ESAC), Science Operations Department, E-28691 Villanueva de la Cañada, Madrid, Spain*
[2]*Tuorla Observatory, University of Turku, Väisäläntie 20, FI-21500 Piikkiö, Finland*
[3]*Nordita, KTH Royal Institute of Technology and Stockholm University, Roslagstullsbacken 23, SE-10691 Stockholm, Sweden*
[4]*Department of Physics and McGill Space Institute, McGill University, 3600 rue University, Montreal, QC H3A2T8, Canada*
[5]*Institut für Astronomie und Astrophysik, Kepler Center for Astro and Particle Physics, Universität Tübingen, Sand 1, D-72076 Tübingen, Germany*
[6]*Kazan (Volga region) Federal University, Kremlevskaya str. 18, Kazan 420008, Russia*

ABSTRACT

When neutron stars (NS) accrete gas from low-mass binary companions, explosive nuclear burning reactions in the NS envelope fuse hydrogen and helium into heavier elements. The resulting thermonuclear (type-I) X-ray bursts produce energy spectra that are fit well with black bodies, but a significant number of burst observations show deviations from *Planck* spectra. Here we present our analysis of *RXTE*/PCA observations of X-ray bursts from the NS low-mass X-ray binary HETE J1900.1-2455. We have discovered that the non-Planckian spectra are caused by photoionization edges. The anticorrelation between the strength of the edges and the colour temperature suggests that the edges are produced by the nuclear burning ashes that have been transported upwards by convection and become exposed at the photosphere. The atmosphere model fits show that occasionally the photosphere can consist entirely of metals, and that the peculiar changes in blackbody temperature and radius can be attributed to the emergence and disappearance of metals in the photosphere. As the metals are detected already in the Eddington-limited phase, it is possible that a radiatively driven wind ejects some of the burning ashes into the interstellar space.

Key words: accretion, accretion discs – X-rays: bursts.

1 INTRODUCTION

The discovery of thermonuclear (type-I) X-ray bursts more than 40 yr ago (Grindlay et al. 1976) opened a new window to study neutron stars (NS). The fuel that powers an X-ray burst comes from a low-mass companion star, from which the NS accretes gas through an accretion disc. For specific ranges of the mass accretion rate (e.g. Fujimoto, Hanawa & Miyaji 1981), unstable nuclear burning can occur producing elements up to tellurium (Schatz et al. 2001). The energy released in the burning escapes as thermal X-ray emission from the NS photosphere (i.e. the X-ray burst), and a fraction of the energy may be spent by ejecting the NS envelope in a wind during the super-Eddington phase (e.g. Paczynski & Proszynski 1986).

The four decades of observations have shown that most X-ray burst energy spectra resemble black bodies (Lewin, van Paradijs & Taam 1993). Correspondingly, NS atmosphere models predict spectral shapes that are well described by a diluted blackbody (e.g. London, Taam & Howard 1986; Suleimanov, Poutanen & Werner 2012), as long as the atmospheres are hot and/or metal-poor (Nättilä

et al. 2015). Since the earliest observations in the 1970s (e.g. Hoffman, Cominsky & Lewin 1980), for some X-ray bursts, the blackbody model fails to fit the spectra in certain sections of the burst (e.g. van Paradijs et al. 1990; Kuulkers et al. 2002; in 't Zand & Weinberg 2010). While some of these discrepancies can also originate from variations of the persistent spectrum during the bursts, there remains a considerable fraction of bursts where more complex spectral descriptions are needed (Worpel, Galloway & Price 2015). By adding photoionization edges to the blackbody model, one can achieve acceptable fits, but it is often difficult to be certain if these features are formed in the NS photosphere (in 't Zand & Weinberg 2010) or by reflecting the X-ray burst emission from the surrounding accretion disc (Strohmayer & Brown 2002; Keek et al. 2014).

One of the peculiar bursts where the blackbody model clearly does not fit the data was observed from HETE J1900.1-2455 by the *Rossi X-ray Timing Explorer* (*RXTE*) on 2005 July 21. Galloway, Morgan & Chakrabarty (2008b) showed that the spectral fits can be improved by including Comptonization and a variable local absorption column in the model. Here we show that the spectra are naturally explained if there is a high metal fraction at the photosphere, consistent with the hypothesis of Weinberg, Bildsten

⋆E-mail: jkajava@sciops.esa.int

& Schatz (2006), who discussed how nuclear burning ashes can rise up towards the photosphere by strong convection, that is also seen in recent multidimensional hydrodynamical simulations (Malone et al. 2011, 2014; Zingale et al. 2015). At the same time, the outer H/He-rich NS envelope can be ejected, ultimately revealing the burning ashes. The high iron abundance in the ashes is a likely reason for appearance of the edges in the spectra (see also in 't Zand & Weinberg 2010) and, additionally, the metals change the photospheric opacity (Nättilä et al. 2015) that leads to the peculiar variations in the blackbody radius and temperature.

2 OBSERVATIONS AND SPECTRAL MODELS

HETE J1900.1-2455 was discovered on 2005 June 14, and follow-up observations revealed it to be a 377 Hz accreting millisecond pulsar in a 83.3 min binary orbit (Kaaret et al. 2006; Suzuki et al. 2007). The pulsations were seen only intermittently, and the pulse amplitudes tended to increase right after X-ray bursts were observed (Galloway et al. 2007). The magnetic field may have been buried by the accretion flow, causing the pulsations to cease within a few months from the discovery (Patruno 2012). X-ray burst oscillations close to the pulsar's spin frequency were seen only in one observation when the source was in the soft spectral state in 2009 (Watts et al. 2009). The optical counterpart is a low-mass star ($M_c \lesssim 0.1$ $M_\odot$) with clear hydrogen emission lines, and the binary inclination is $i \lesssim 20°$ (Elebert et al. 2008). The distance to the source d lies in the range 3.0–5.5 kpc (Galloway et al. 2008a), and we assume here $d = 4.2$ kpc, in the middle of the proposed range.

In this Letter, we report our analysis of the 10 X-ray bursts of HETE J1900.1-2455 that have been observed by the *RXTE* satellite (see Kajava et al. 2014, table A1), mainly concentrating on the most energetic 2005 July 21 burst (Burst 1 hereafter). We performed time-resolved X-ray spectral modelling of the Proportional Counter Array (PCA; Jahoda et al. 2006) data in the 3–20 keV energy range. The observations were split into 0.25–2 s time segments. Initially, the net burst spectra were fitted in XSPEC (Arnaud 1996) with a blackbody model BBODYRAD, characterized by a temperature T_{bb} and a normalization $K = (R_{bb} \text{[km]}/d_{10})^2$, where R_{bb} is the blackbody radius and d_{10} is the distance in units of 10 kpc. Absorption by the interstellar medium was taken into account using the TBABS model (with fixed hydrogen column density $N_H = 0.16 \times 10^{22}$ cm^{-2}; Worpel, Galloway & Price 2013). These data were also analysed in Kajava et al. (2014), where the standard data reduction methods are described.

We additionally fitted the Burst 1 with our atmosphere model MATMOS (Nättilä et al. 2015). The main model assumption is that the NS photosphere coincides with the NS surface, which is why we fit the model only in the cooling phase of the X-ray burst. Stellar rotation is not considered here; this causes the photoionization edges to be (artificially) sharp features in the modelling, but the expected Doppler broadening is not larger than the spectral resolution. MATMOS has two free parameters; the normalized atmospheric luminosity g_{rad}/g and the 'metal enhancement factor' ζ. g_{rad}/g is the ratio of the radiative acceleration and surface gravity, where the value of unity corresponds to the Eddington limit. ζ is defined as the factor by which metal abundances of Asplund et al. (2009) are increased, after which hydrogen and helium abundances are scaled down in solar ratios. For the solar composition, $\zeta \equiv 1$, and for an atmosphere consisting of metals only, $\zeta \approx 70$. The MATMOS model normalization is $A = (R_\infty/d)^2$, where $R_\infty = R_{NS}(1 + z)$ is the apparent NS radius as seen by a distant observer and $1 + z = (1 - 2GM_{NS}/R_{NS}c^2)^{-1/2}$ is the gravitational redshift at the NS surface. We implicitly assume

an NS radius of $R_{NS} = 12$ km and a mass of $M_{NS} = 1.4 \, M_\odot$ and, therefore, with the constant distance of 4.2 kpc, A is not allowed to vary in the modelling. Our choice of NS radius and mass then also determines the gravitational redshifts of the photoabsorption edges, which we find are well fit with this choice of NS mass and radius. A more detailed analysis exploring the constraints on mass, radius and distance will be presented in a forthcoming letter. MATMOS model parameter minimization was performed in a Bayesian framework using the Metropolis–Hastings algorithm within the Markov Chain Monte Carlo method.

3 SPECTRAL ANALYSIS

The parameter time evolution resulting from the blackbody spectral modelling is shown in Fig. 1 for the first and most energetic X-ray burst from HETE J1900.1-2455 (Burst 1), observed on 2005 July 21 (MJD 53572). As noted by Galloway et al. (2008b), the light curve of this X-ray burst is highly atypical. The burst rise-time from the persistent flux level $F_{per} \approx 0.7 \times 10^{-9}$–$F_{bb} \approx 10^{-7}$ erg cm^{-2} s^{-1} was only about 30 ms, which is then followed by a 30 per cent flux drop in the next 2 s. The subsequent increase of the flux (black line in Fig. 1a) is accompanied by a decreasing blackbody temperature (red line) and an increasing blackbody radius (blue line), indicating that the photosphere lifts off from the NS surface. The radius expansion halts about 15 s into the burst, where the F_{bb} and R_{bb} attain two local maxima, while T_{bb} simultaneously attains two local minima. During the next 18 s, the photosphere slowly contracts back towards the NS surface, finally reaching it at 34 s from the start of the burst. This marks the photospheric 'touchdown', where T_{bb} reaches a local maximum and R_{bb} a local minimum. At the same time, the flux decays from $F_{PRE} \approx 1.36 \times 10^{-7}$ to $F_{TD} \approx 1.23 \times 10^{-7}$ erg cm^{-2} s^{-1} during this photospheric radius expansion (PRE) phase. The cooling phase of the burst has two very distinct phases. The initial cooling phase from 34 s onwards shows a smooth flux decay with a gradual increase of the radius. Then around 48 s, the temperature increases significantly while simultaneously R_{bb} abruptly drops within 3 s. This transition is accompanied by clear flux fluctuations on top of the power law-type decay (with an index of $\gamma = 1.74 \pm 0.02$, see Fig. 1a, green dashed line). Afterwards, R_{bb} remains constant while the temperature evolves more slowly than in the initial phase.

The blackbody model is a poor description of the data in two localized parts in the radius expansion- and the cooling phase (Fig. 1f). Similarly to in 't Zand & Weinberg (2010), we find that by adding a photoabsorption edge to the model (EDGE in XSPEC), the fits are improved significantly (Figs 1d–f). The addition of an EDGE does not change the blackbody temperature or radius significantly (pink and magenta lines in Figs 1b and 1c). For this burst, the edges appear significant only when the blackbody temperature is below about 2.2 keV (grey bands in Fig. 1). Furthermore, the edge optical depth varies in the range of $\tau_{edge} \approx 0.2$–0.6 and it is anticorrelated with the blackbody temperature. We also find that the edge energies are higher in the radius expansion phase as compared to the cooling phase, 8.07 ± 0.08 and 7.62 ± 0.09 keV, respectively. The variable edge energy and depth, and their direct dependency upon the blackbody temperature (and not with the ionizing flux), strongly imply that the edges are produced in the stellar photosphere, rather than by reflecting the burst emission from the surrounding accretion disc. The likely cause for the temperature dependency is that at higher temperatures (around touchdown), iron is fully ionized in the NS photosphere, and only at lower temperatures, iron can recombine to create photoionization edges to the spectra (Nättilä et al. 2015).
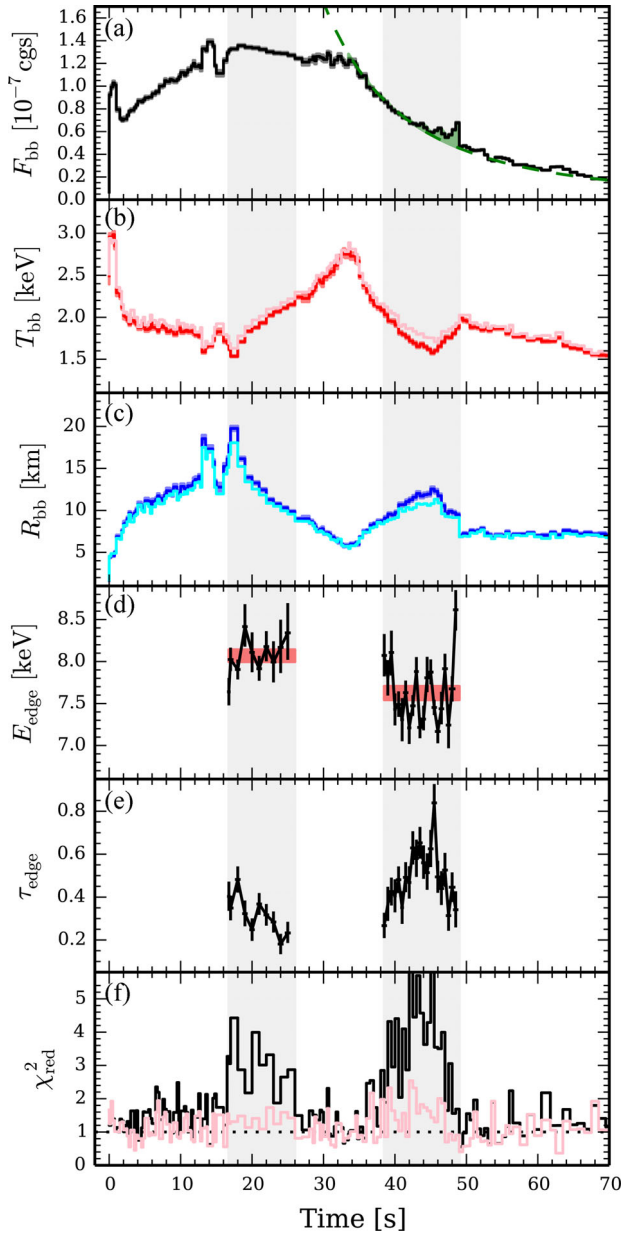
Figure 1. Time evolution of the best-fitting spectral parameters in Burst 1. (a) Blackbody flux (the green line shows a power-law flux decay fit), (b) blackbody temperature (red for BB and pink for BB + EDGE model), (c) blackbody radius assuming $d = 4.2$ kpc (blue for BB and cyan for BB + EDGE model), (d) photoionization edge energy, (e) edge optical depth and (f) reduced χ^2 of the fits (black for BB model and pink for the BB + EDGE model). The width of the lines in panels (a)–(c) denote the 1σ errors.

To study the edges, we fitted the cooling phase spectra with the atmosphere model MATMOS (see Figs 2 and 3). The normalized atmospheric luminosity, g_{rad}/g, decreases in a similar fashion as the blackbody flux, displaying the same flux fluctuations towards the end of the cooling phase. The most remarkable feature is the metal enhancement factor, which is initially higher than about $\zeta \approx 50$ and it is consistent with the maximum value of $\zeta \approx 70$ where the atmosphere consists entirely of metals (i.e. no H nor He). Then, around 48 s after the burst onset, the metal content drops towards the solar value $\zeta \approx 1$ in about 3 s. The MATMOS model gives a far better description of the data, $\chi^2_{red} \approx 1.2$, compared to $\chi^2_{red} \gtrsim 3$ in
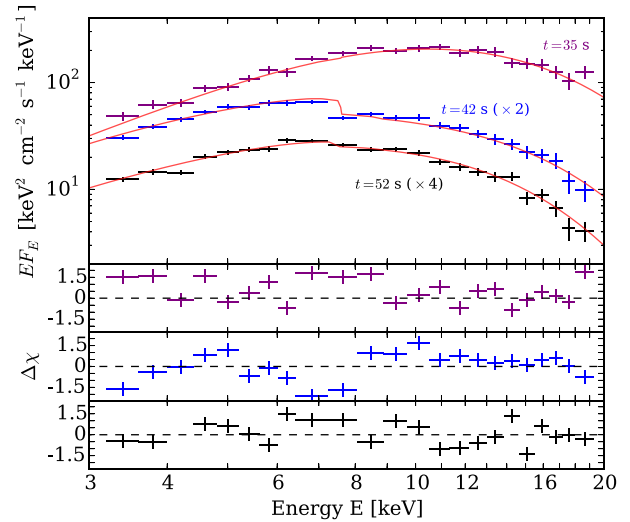

Figure 2. EF_E spectra of HETE J1900.1-2455 X-ray burst 1 modelled with the MATMOS atmosphere in three phases in the cooling tail.
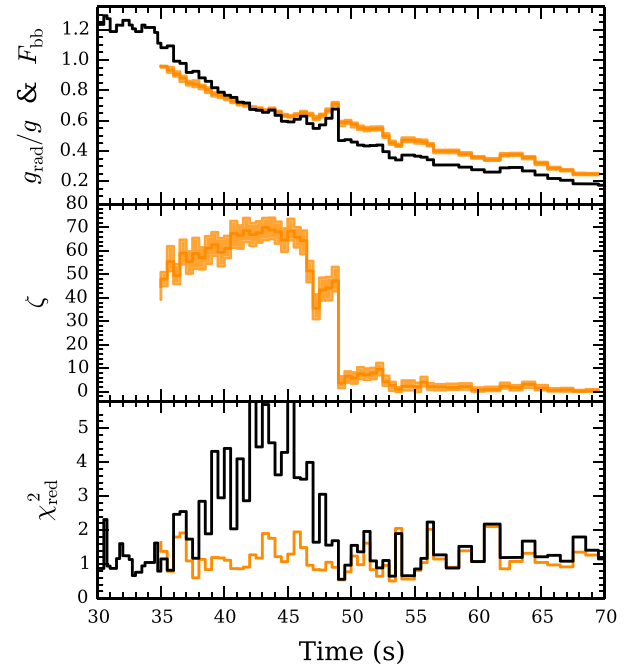
Figure 3. MATMOS model fits for the cooling phases with a variable chemical composition (orange lines). Top panel: the normalized atmospheric luminosity, g_{rad}/g, that decays similarly to the blackbody flux (black lines in units of 10^{-7} erg cm^{-2} s^{-1}). Middle panel: metal enhancement factor ζ. Bottom panel: the reduced χ^2 for the MATMOS and BBODYRAD models.

the blackbody fits with the same number of free parameters (see Fig. 3).

The atmosphere modelling shows that the edge is mainly produced by H-like Fe ions at $E_{FeXXVI} = 9.28$ keV, gravitationally redshifted to 7.62 keV. While only H-like iron contributes significant edges in the 3–20 keV range, the other metals impact the spectra in a more indirect way. The metals increase the photospheric electron density and the bound-free and free–free opacities, pushing the spectral colour-correction factor – defined as the ratio between the colour and the effective temperatures $f_c \equiv T_c/T_{eff}$ – to lower values with respect to solar abundances (Nättilä et al. 2015). Therefore, the
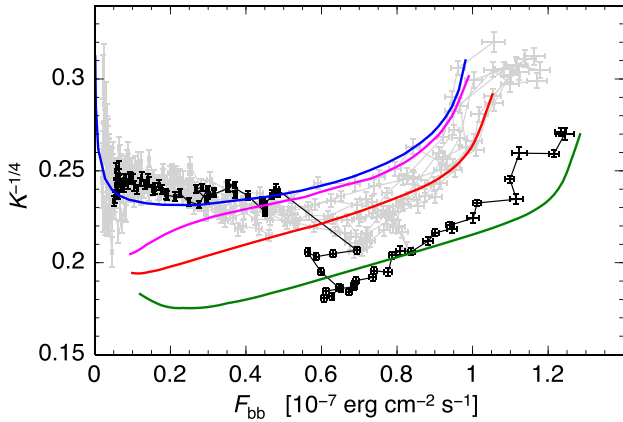
Figure 4. Blackbody normalization versus the flux of HETE J1900.1-2455 bursts together with the colour correction curves, f_c, for an $M_{NS} = 1.4\,M_{\odot}$ and $R_{NS} = 12$ km NS. The track from Burst 1 is highlighted with black colour. The blue, purple, red and green lines are for MATMOS f_c curves with metal enhancement factors $\zeta = 0.01, 1, 10$ and 40, respectively.

drop in the metal enhancement causes the colour-correction factor to jump from $f_c \approx 1.1$ to 1.4, which results in the observed blackbody temperature and radius variations in Fig. 1 around 48 s, given the dependence $R_{bb} = R_{NS}(1 + z)f_c^{-2}$ (Lewin et al. 1993).

Other X-ray bursts have been observed from HETE J1900.1-2455, which also could have exhibited similar metal-induced variations in f_c, that would be imprinted as a scatter in the observed blackbody radii. Therefore, we compare the emission areas during the cooling tails of all hard state X-ray bursts from HETE J1900.1-2455 in Fig. 4, in the so-called l–f_c diagram (equivalently F–$K^{-1/4}$ diagram). This is a convenient way to compare many X-ray bursts to atmosphere models, because of the relation $f_c \propto K^{-1/4}$ (Lewin et al. 1993; Suleimanov et al. 2011). In Fig. 4, Burst 1 is highlighted with black symbols, while the other seven bursts which occurred in the hard state are shown with grey symbols. The discrepant evolution of the soft- and intermediate-state bursts – likely due to the spreading layer in the disc–NS boundary (Suleimanov et al. 2011; Poutanen et al. 2014; Koljonen, Kajava & Kuulkers 2016) – is not shown in Fig. 4; such bursts start with a constant normalization, and then show a large drop at lower fluxes, similarly to the soft state bursts of 4U 1636-536 (Zhang, Méndez & Altamirano 2011) and 4U 1608-52 (Poutanen et al. 2014). The blue line shows the theoretical $\zeta = 0.01$ f_c-curve, which is in good agreement with the data for the bursts at fluxes below ~50 per cent of the Eddington value. At higher fluxes, the bursts gradually deviate from the low-metallicity f_c-curves, each becoming more consistent with moderately enhanced atmospheres ($\zeta = [1–10]$; purple and red lines). Burst 1, clearly standing out as the most extreme case, is initially closer to the $\zeta = 40$ curve and then jumps up to values consistent with solar to sub-solar tracks during the transition in the cooling phase. Interestingly, most of the bursts are consistent with metal enhanced ($\zeta = [1–10]$) f_c-curves closer to the touchdown flux, and they all tend to follow the sub-solar curves below $F_{bb} \lesssim 4 \times 10^{-8}$ erg cm^{-2} s^{-1}.

4 DISCUSSION

The appearance of edges 14 s after the burst onset likely marks the time when the outer H/He-rich envelope is ejected in the wind (Weinberg et al. 2006). Based on the light-curve models of in 't Zand & Weinberg (2010) the fact that the bursts stayed above Eddington luminosity for more than 30 s implies an ignition column $y \approx 2 \times 10^9$ g cm^{-2}. This can be accumulated in about 16 d with the

persistent accretion rate observed prior to the X-ray burst (roughly 2 per cent of Eddington), matching well with the HETE-2 detection of a previous X-ray burst 14 d earlier (Suzuki et al. 2007). At these low accretion rates, stable hydrogen burning likely built up a large He pile (Galloway & Cumming 2006), consistent with the strong radius expansion. The expected wind mass-loss rate is $\dot{M}_w \sim 10^{18}$ g s^{-1} (Paczynski & Proszynski 1986; Weinberg et al. 2006) which, in 14 s, can eject a mass $M_w > 10^{19}$ g. This matches the column of $y_w \approx 10^6$ g cm^{-2} that must be ejected to expose ashes, set by the maximum extent of the convection zone during the flash (Weinberg et al. 2006). Thus, the deep ignition and the unusually long PRE-phase likely provided the necessary conditions for the convection to extend sufficiently far out towards the photosphere. In the subsequent 18 s 'metal-enriched wind phase' the total mass loss is also $\Delta M_z \sim 10^{19}$ g, which, according to the MATMOS model results, consists largely of metals. The large He fraction before ignition (Falanga et al. 2007) means a low proton abundance which suggests that significant rp-process burning did not occur in this burst (Weinberg et al. 2006). Therefore, it remains unclear if the rp-process contributes to the Galactic metal enrichment (Schatz et al. 1998).

When the temperature was below about $\lesssim 2.2$ keV, photo-absorption edges appeared both in the Eddington-limited phase and in the cooling phase, and the edge energies decreased from 8.07 ± 0.08 to 7.62 ± 0.09 keV, respectively. Our atmosphere models showed that in the cooling phase the dominant ion that produces the photo-ionization edge is H-like Fe at $E_{FeXXVI} = 9.28$ keV, although other weaker features are also present. This energy shift $E_{Fe\,XXVI}/E_{edge} \approx 1.22$ is consistent with the gravitational redshift at the NS surface, $1 + z \approx 1.24$, for the assumed $M_{NS} = 1.4\,M_{\odot}$ and $R_{NS} = 12$ km. In the Eddington limited phase the redshift is instead $1 + z_{PRE} \approx 1.15$. The measured redshift difference can then be used to estimate how much the photosphere expanded during the Eddington-limited phase. We find that the radius where the edge is formed is about $R_{PRE} \approx 17$ km, i.e. the radius expansion was roughly 5 km. Note also that a similar redshift variation can be derived from the relation $F_{PRE}(1 + z_{PRE})^2 = F_{TD}(1 + z_{TD})^2$ (e.g. Lewin et al. 1993), which assumes that in the radius expansion phase the flux is always the local Eddington flux. Furthermore, given that $R_{bb} = R_{NS}(1 + z)f_c^{-2}$ (Lewin et al. 1993), we can also estimate the colour correction factor during the radius expansion phase. At touchdown, we have measured $1 + z_{TD} \approx 1.22$, $R_{bb,\,TD} \approx 5.5$ km and taking $R_{NS} = 12$ km we obtain $f_{c,\,TD} \approx 1.63$, which is consistent with highly metal enriched atmosphere models near the Eddington flux (Nättilä et al. 2015). In the radius expansion phase, we can use the estimated $1 + z_{PRE} \approx 1.15$, $R_{bb,\,PRE} \approx 16.3$ km (at 19 s after the burst onset) and $R_{PRE} \approx 17$ km to find that $f_{c,\,PRE} \approx 1.10$. The ratio $f_{c,\,PRE}/f_{c,\,TD} \approx 0.67$ (independent of distance), is similar to the values found in the cooling tail before the transition at ~50 per cent of the Eddington flux. The presence of strong photo-ionization edges in cooler photosphere in both cases likely reduces the colour correction factor to the same value, but accurate radiative transfer calculations for expanding, wind launching NS atmospheres are needed to confirm this.

In Fig. 1(a), the flux enhancements between 46–49 s after the burst onset have an excess fluence of about 3.9×10^{-8} erg cm^{-2} above the power-law decay (indicated by the green hatched area in Fig. 1). The strong radius expansion likely halted accretion on to the NS before this time, and the "missing" persistent emission fluence accumulated would have been about 3.3×10^{-8} erg cm^{-2}. The match between these fluences suggests that the flux excess in the tail is caused by accreting the accumulated gas that was

halted by the X-ray burst. Therefore, the transition to the second cooling phase in the X-ray burst was likely caused by covering the metal-rich NS photosphere with fresh, H/He-rich layer from the accretion disc. The ∼10 s duration of the metal-rich cooling stage allowed the photosphere to cool enough to reveal the ashes as strong photoabsorption edges. This was likely facilitated by the unusually long PRE-phase, during which the accretion disc was pushed a few km backwards by the X-ray burst. In other bursters (and in the other HETE J1900.1-2455 bursts) with shorter PRE-phases and/or weaker magnetic fields, the NSs may be covered by an H/He-rich layer before the photosphere cools enough, and thus they may not have as obvious non-Planckian spectra.

The detection of burning ashes in HETE J1900.1-2455, and likely in other bursters (in 't Zand & Weinberg 2010), has several consequences. We have found evidence that the burning ashes should get convectively mixed in the NS envelope during X-ray bursts (as simulations suggest), and that NSs should have significant mass-loss during radius-expansion episodes. More detailed modelling will involve coupling burst models which follow convection and nuclear burning (e.g. Woosley et al. 2004) to models of super-Eddington winds (Paczynski & Proszynski 1986). Also, input from nuclear experiments is important to include in nuclear networks to make accurate predictions of the ash composition (Weinberg et al. 2006). Another consequence is related to the observed R_{bb} scatter and the touchdown flux scatter seen in several bursters (Güver, Psaltis & Özel 2012a; Güver, Özel & Psaltis 2012b), which can be caused by the variable metal enhancement in different X-ray bursts. At least for HETE J1900.1-2455, judging from Fig. 4, most of the PRE-bursts show signs of photospheric metal enhancement, and thus the nuclear burning ashes may reach the NS photospheres much more commonly than previously thought. In these cases one must be careful in deriving NS M–R constraints from X-ray burst observations using blackbodies and colour correction factors: it is not obvious that the typical X-ray burst is one where no metal enhancement is present (compare, e.g. Suleimanov et al. 2011; Nättilä et al. 2016). The ashes may lead to systematic uncertainties in NS radii by up to 4 km (see Poutanen et al. 2014, fig. 7). On the other hand, the photoabsorption edges, where present, provide an independent M–R constraint, but that requires fitting the atmosphere models directly to the observed spectra. For better measurements of edges for bursts with more modest metal enhancements (and of other elements than iron), an observatory like the *LOFT* (see e.g. in 't Zand et al. 2015) would be needed. Meanwhile, analysis of archival data sets should give us a better handle on how frequently, and under which conditions, the edges can be detected.

ACKNOWLEDGEMENTS

REFERENCES

Arnaud K. A., 1996, in Jacoby G. H., Barnes J., eds, ASP Conf. Ser. Vol. 101, ADASS V. Astron. Soc. Pac., San Francisco, p. 17

Asplund M., Grevesse N., Sauval A. J., Scott P., 2009, ARA&A, 47, 481

Elebert P., Callanan P. J., Filippenko A. V., Garnavich P. M., Mackie G., Hill J. M., Burwitz V., 2008, MNRAS, 383, 1581

Falanga M., Poutanen J., Bonning E. W., Kuiper L., Bonnet-Bidaud J. M., Goldwurm A., Hermsen W., Stella L., 2007, A&A, 464, 1069

Fujimoto M. Y., Hanawa T., Miyaji S., 1981, ApJ, 247, 267

Galloway D. K., Cumming A., 2006, ApJ, 652, 559

Galloway D. K., Morgan E. H., Krauss M. I., Kaaret P., Chakrabarty D., 2007, ApJ, 654, L73

Galloway D. K., Muno M. P., Hartman J. M., Psaltis D., Chakrabarty D., 2008a, ApJS, 179, 360

Galloway D. K., Morgan E. H., Chakrabarty D., 2008b, in Wijnands R. et al., eds, AIP Conf. Proc. Vol. 1068, A Decade of Accreting Millisecond Pulsars. AIP, Melville, NY, p. 55

Grindlay J., Gursky H., Schnopper H., Parsignault D. R., Heise J., Brinkman A. C., Schrijver J., 1976, ApJ, 205, L127

Güver T., Psaltis D., Özel F., 2012a, ApJ, 747, 76

Güver T., Özel F., Psaltis D., 2012b, ApJ, 747, 77

Hoffman J. A., Cominsky L., Lewin W. H. G., 1980, ApJ, 240, L27

in 't Zand J. J. M., Weinberg N. N., 2010, A&A, 520, A81

in 't Zand J. J. M. et al., 2015, preprint (arXiv:1501.02776)

Jahoda K., Markwardt C. B., Radeva Y., Rots A. H., Stark M. J., Swank J. H., Strohmayer T. E., Zhang W., 2006, ApJS, 163, 401

Kaaret P., Morgan E. H., Vanderspek R., Tomsick J. A., 2006, ApJ, 638, 963

Kajava J. J. E. et al., 2014, MNRAS, 445, 4218

Keek L., Ballantyne D. R., Kuulkers E., Strohmayer T. E., 2014, ApJ, 797, L23

Koljonen K. I. I., Kajava J. J. E., Kuulkers E., 2016, preprint (arXiv:1606.00595)

Kuulkers E., Homan J., van der Klis M., Lewin W. H. G., Méndez M., 2002, A&A, 382, 947

Lewin W. H. G., van Paradijs J., Taam R. E., 1993, Space Sci. Rev., 62, 223

London R. A., Taam R. E., Howard W. M., 1986, ApJ, 306, 170

Malone C. M., Nonaka A., Almgren A. S., Bell J. B., Zingale M., 2011, ApJ, 728, 118

Malone C. M., Zingale M., Nonaka A., Almgren A. S., Bell J. B., 2014, ApJ, 788, 115

Nättilä J., Suleimanov V. F., Kajava J. J. E., Poutanen J., 2015, A&A, 581, A83

Nättilä J., Steiner A. W., Kajava J. J. E., Suleimanov V. F., Poutanen J., 2016, A&A, 591, A25

Paczynski B., Proszynski M., 1986, ApJ, 302, 519

Patruno A., 2012, ApJ, 753, L12

Poutanen J., Nättilä J., Kajava J. J. E., Latvala O.-M., Galloway D. K., Kuulkers E., Suleimanov V. F., 2014, MNRAS, 442, 3777

Schatz H. et al., 1998, Phys. Rep., 294, 167

Schatz H. et al., 2001, Phys. Rev. Lett., 86, 3471

Strohmayer T. E., Brown E. F., 2002, ApJ, 566, 1045

Suleimanov V., Poutanen J., Revnivtsev M., Werner K., 2011, ApJ, 742, 122

Suleimanov V., Poutanen J., Werner K., 2012, A&A, 545, A120

Suzuki M. et al., 2007, PASJ, 59, 263

van Paradijs J., Dotani T., Tanaka Y., Tsuru T., 1990, PASJ, 42, 633

Watts A. L. et al., 2009, ApJ, 698, L174

Weinberg N. N., Bildsten L., Schatz H., 2006, ApJ, 639, 1018

Woosley S. E. et al., 2004, ApJS, 151, 75

Worpel H., Galloway D. K., Price D. J., 2013, ApJ, 772, 94

Worpel H., Galloway D. K., Price D. J., 2015, ApJ, 801, 60

Zhang G., Méndez M., Altamirano D., 2011, MNRAS, 413, 1913

Zingale M., Malone C. M., Nonaka A., Almgren A. S., Bell J. B., 2015, ApJ, 807, 60

This paper has been typeset from a TeX/LaTeX file prepared by the author.